

**UNDERSTANDING TRI-REFORMING OF METHANE
USING HYDROTALCITE-DERIVED CATALYSTS
FOR UTILIZATION OF CO₂ OF FLUE GASES FROM
THERMAL POWER PLANTS**

ROHIT KUMAR



DEPARTMENT OF CHEMICAL ENGINEERING
INDIAN INSTITUTE OF TECHNOLOGY DELHI

APRIL 2021

©Indian Institute of Technology Delhi (IITD), New Delhi, 2021

**UNDERSTANDING TRI-REFORMING OF METHANE
USING HYDROTALCITE-DERIVED CATALYSTS
FOR UTILIZATION OF CO₂ OF FLUE GASES FROM
THERMAL POWER PLANTS**

by

Rohit Kumar

Department of Chemical Engineering

Submitted

in fulfilment of the requirements for the award of the degree of Doctor of Philosophy

to the



INDIAN INSTITUTE OF TECHNOLOGY DELHI

APRIL 2021

DEDICATED

TO

MY FAMILY

CERTIFICATE

This is to certify that the thesis entitled, “**UNDERSTANDING TRI-REFORMING OF METHANE USING HYDROTALCITE-DERIVED CATALYSTS FOR UTILIZATION OF CO₂ OF FLUE GASES FROM THERMAL POWER PLANTS**” being submitted by **Mr. ROHIT KUMAR** to the Indian Institute of Technology, Delhi for the award of DOCTOR OF PHILOSOPHY is a record of bonafide research work carried out by him under guidance and supervision in conformity with the rules and regulations of Indian Institute of Technology, Delhi.

The research report and results presented in this thesis have not been submitted, in part or full, to any other university or institute for the award of ant degree or diploma.



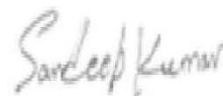
(K. K. Pant)

Professor
Department of Chemical Engineering
Indian Institute of Technology, Delhi
New Delhi – 110016
India



(N. V. Choudary)

Scientist Emeritus
Hindustan Petroleum Green R&D Centre
Bengaluru, Karnataka
India



(Sandeep Kumar)

Professor
Department of Civil & Environmental Engineering
Old Dominion University, Virginia
United States of America

ACKNOWLEDGMENTS

*With deep gratitude, it gives me colossal pleasure to thank my supervisor and mentor **Prof. K. K. Pant**, Department of Chemical Engineering, IIT Delhi, for his unconditional support, forbearance, motivation, enthusiasm, and immense knowledge that guided me to uphill the daunting task of research in my PhD. His unwavering enthusiasm and scientific keenness not only kept me constantly engrossed with my research but also helped me develop an understanding of the subject. His personal munificence made my life at IIT Delhi a wonderful and enjoyable experience. He has always motivated me to realize my potential and helped me to develop new ideas to pursue my research work. He has always been quick in providing me his comments on manuscripts, reports and ppt presentations. Also, I am lucky enough to have him anytime to discuss research projects or any personal issues.*

*I express my deep gratitude to my co-supervisor **Dr. N. V. Choudary**, HP Green R&D centre, Bengaluru for his unconditional guidance and support throughout my PhD. The technical discussions with him always motivated me to pursue high quality research work. Dr. Choudary's industrial experience helped me in being familiar with the thought process of industrial researchers on a research problem. I am really thankful to him for his genuine interest in my professional and personal growth.*

*My special words of thanks also go to my co-supervisor **Prof. Sandeep Kumar**, Department of Civil and Environmental Engineering, Old Dominion University, USA. His expertise in process and catalysis nurtured me as a researcher. I owe him lots of gratitude for making me learn how to approach a research problem. I am really glad to be associated with a person like him in my life.*

*I am profoundly thankful to my SRC committee comprising **Prof. Sreedevi Upadhyayula**, **Prof. M. Ali Haider** and **Prof. Ravi P. Singh**. Their critical reviews and important suggestions during my SRC presentations helped me in gaining insights into my research area. These presentations always pushed me to come up with more clarity and concepts on my research topic. The SRC committee has directly or indirectly increased my interest in research. I wish to convey my sincere thanks to them.*

I am thankful to IIT Delhi, DST and CSIR for funding my international conferences at Belgium, Australia and Germany respectively. I found it a great platform where I can interact with the people around the world working in my research area.

I express my gratitude to the department of Chemical Engineering, IIT Delhi for providing me the XRD instrumental facility. The central research facility (CRF) and SMITA labs of IIT Delhi were kind enough to me for carrying out TEM, SEM, Raman, SAXS measurements.

*I express my gratitude to **Mr. Manish Mishra** (Centurion Scientific) for helping me with his expertise whenever GC equipped with TCD instrument failed to perform correctly. I am thankful to **Mr. Vishesh Kumar Yadav**, lab-in-charge for helping me in purchasing works related to my PhD project. I thank **Mr. Krishan Kumar** for helping me with computer's software, hardware and internet related issues. **Mr. Suchit Kumar Pal** have helped me in experimental works. I am thankful to him also.*

*I and **Mr. Kritagya Kumar** performed some of experiments together in initial phase of my PhD. He also helped in proofreading of our manuscripts. I am thankful to him for all these co-operation. **Mr. V.B.S.S. Reddy** helped me in kinetic modeling part of my thesis. He had been busy with academic work of his master's degree, which he was pursuing in France. Despite this, several late night discussion with him really helped in completing kinetic modeling work. For this, I am grateful to him. A number of technical discussions with my lab-mates **Dr. Sonal, Mr. Sonit Balyan, Mr. Sourabh Mishra, Mr. Kaushal Parmar, Mr. Prashant Jadhao** and **Ms. Uma Dwivedi** cleared my some of technical doubts. I must mention Mr. Sonit Balyan for helping me in preparing graphical abstracts of the manuscripts. Also, Mr. Prashant Jadhao, Mr. Sourabh Mishra and Dr. Sonal used to switch off my experimental reactor set-up at nights when the reactor used to get cooled enough for closing after the completion of reaction. I am especially thankful to Mr. Sourabh Mishra for appreciating my research aptitude and knowledge. His appreciation has always pushed me to improve the quality of my research work. I am grateful to other lab-mates **Mr. Akshay Mankar, Mr. Rajan Singh, Ms. Komal Tripathi** and **Mr. Ramdayal Panda** along with those mentioned above for keeping lab environment friendly. I have always lab group presentations and found it a great forum among ourselves to gain knowledge and discuss various stuff including lab activity. I am thankful to **Mr. Prateek Khatri, Ms. Shreya Singh, Ms. Snigdha Mishra** and **Ms. Komal Sharma** for their word of appreciation on my research work. A special mention to **Dr. Ashish Pandey**, who joined our lab when I was pretty much in writing stage. He has been a great company to me and his advice helped in some or other way. I must mention **Dr. Sonal Ashthana** here as I cannot forget the proofreading and technical writing corrections she used to do for some of my manuscripts. Apart from these two, some other post-doctoral fellows of our lab **Dr. Dinesh Gupta, Dr. Chandrakant Mukesh** and **Dr. Tapas Dora** helped me with their knowledge whenever I asked for.*

*My parents have motivated me throughout my PhD degree. Their concern and constant support was unmatched and inspired me to pursue PhD in an ideal manner. I am very much grateful to my younger brothers **Mr. Mohit Kumar** and **Mr. Rajat Kumar** for their constant encouragement throughout my PhD. I am also very thankful to my dear wife **Ms. Sonam Jaiswal** for her support during my PhD. She has always remained calm and patient about the completion of my PhD degree.*

Herewith I would like to thank all of those, who have directly or indirectly contributed to the realization of this thesis.

Rohit Kumar

ABSTRACT

The global warming and climate change are the biggest challenges of current century. These are often related to CO₂ emission. The conversion of CO₂ to fuels and chemicals could be an ideal strategy to curb CO₂ emission. In this context, tri-reforming of methane (TRM) is a promising technique. The flue gas from electric power plants are the largest contributor to CO₂ emission. TRM process does not requires pre-separation of CO₂ from flue gas. In this process, CO₂, H₂O and O₂ of flue gas react with CH₄ to generate synthesis gas. However, the deactivation of catalyst impedes large-scale implementation of TRM. The reforming catalysts tend to deactivate due to carbon deposition, active metal sintering and active metal oxidation. The high activity and stability of catalyst are the major challenges of TRM. The research work presented in this thesis aims to develop a highly active and stable catalyst for TRM reaction for utilization of industrial flue gas.

The support phase of a catalyst has significant influence on catalyst performance. Various metal oxides (Al₂O₃, SBA-15, ZrO₂, CeO₂-ZrO₂, TiO₂ and MgO) were used as a support of Ni catalyst. Their performances were compared under identical reaction condition. Based on CH₄ conversion, the initial activity of these catalysts followed the order: Ni/Al₂O₃ > Ni/SBA-15 > Ni/ZrO₂ > Ni/CeO₂-ZrO₂ > Ni/TiO₂ > Ni/MgO. Ni/Al₂O₃ derived from spinel precursor NiAl₂O₄ resulted in well-dispersed smaller Ni particles, stronger metal-support interaction, a higher degree of reducibility and higher basic sites concentration, which led to its superior activity over other catalysts. On the contrary, the stability of SBA-15 and ZrO₂ supported Ni catalysts was remarkably high in 10 h run. Hexagonal porous network of SBA-15 confined Ni particles that resulted in high resistance against metal sintering and carbon deposition whereas Ni/ZrO₂ offered resistance to Ni oxidation owing to its oxophilic property. Experimental investigations reveal that Ni/TiO₂ and Ni/MgO resulted in poor CH₄, CO₂ and H₂O conversions for TRM due to lower degree of reducibility. Furthermore, Ni/CeO₂-ZrO₂ catalyst exhibited lower conversion compared to Ni/Al₂O₃, Ni/SBA-15, and Ni/ZrO₂ due to larger Ni crystallite size.

The role of metal-support interaction (MSI) in the performance of Ni/TiO₂, Ni/SBA-15, Ni/MgO, and Ni/Al₂O₃ catalysts was investigated. To impart weak metal-support interaction (WMSI), the catalysts were calcined at 400°C. While calcination at 850°C or above temperature generated strong metal-support interaction (SMSI) in each catalyst. Ni/SBA-15 and Ni/Al₂O₃

catalysts were calcined at 550°C and 700°C as well to impart medium-strength MSI. The experimental results revealed that Ni/TiO₂ and Ni/MgO catalysts having WMSI (Ni/TiO₂@400 and Ni/MgO@400) displayed high initial activity due to the higher extent of reduction and Ni dispersion. However, these catalysts deactivated during 10 h reaction run. On the other hand, the performances of Ni/TiO₂ and Ni/MgO catalysts having SMSI (Ni/TiO₂@850 and Ni/MgO@850) were unsatisfactory. For Ni/SBA-15 catalyst system, catalysts having weaker MSI (Ni/SBA-15@400, Ni/SBA-15@550 and Ni/SBA-15@700) were more active than the catalyst having stronger MSI (Ni/SBA-15@850). However, the stability of Ni/SBA-15 catalysts was governed by Ni confinement in the pores of SBA-15 rather than the strength of MSI. The activity of Ni/Al₂O₃ catalyst was found to increase with increase in the strength of MSI (Ni/Al₂O₃@400 < Ni/Al₂O₃@550 < Ni/Al₂O₃@700 < Ni/Al₂O₃@950). Ni/Al₂O₃ having SMSI had monodispersed Ni atoms in close association with Al₂O₃, which resulted in higher reforming activity compared to that of Ni/Al₂O₃ having WMSI. Moreover, the deactivation rate was found to decrease with increase in strength of MSI as stronger MSI enhanced Ni/Al₂O₃ catalyst's ability to combat deactivation due to the carbon deposition and Ni metal sintering. The chemical nature of carbon deposits over the Ni/Al₂O₃ catalyst was also observed to be affected by the strength of MSI as it tends to become more graphitic with a decrease in strength of MSI.

Materials derived from hydrotalcite were also explored as a catalyst in TRM reaction. For this study, five catalysts were prepared by co-precipitation method. These were Ni-Mg-Al, Ni-Mg-Al_{me}@500, Ni-Mg-Al_{me}@900, Ni-Cu-Mg-Al and Ni-Zn-Mg-Al. Ni-Mg-Al_{me}@500 and Ni-Mg-Al_{me}@900 were synthesized using memory effect (me) property of hydrotalcite. The non-promoted Ni catalyst, Ni-Mg-Al, displayed lower activity due to the low degree of reducibility. Although by adopting memory effect in preparation of hydrotalcite-derived Ni catalysts, the degree of reducibility was improved and higher initial activity was achieved for Ni-Mg-Al_{me}@500 and Ni-Mg-Al_{me}@900, but these catalysts were vulnerable to deactivation due to Ni oxidation, metal sintering and carbon formation. The addition of Cu resulted in formation of Ni-Cu alloy. It reduced the ensemble size of Ni, which resulted in higher activity and stability as compared to non-promoted Ni catalysts. However, post reaction characterization results revealed Ni oxidation of Ni-Cu-Mg-Al catalyst. The addition of Zn was found more effective in keeping the Ni in its metallic state thereby enhancing its stability. Moreover, the XPS results revealed that Zn addition electronically modified the Ni catalyst by charge transfer phenomenon and made Ni electron rich. As a result, Ni-Zn-Mg-Al catalyst exhibited remarkable tri-reforming activity.

Ni-Zn-Mg-Al catalyst was further studied for TRM by varying its M^{II}/M^{III} ratio and Ni loading. The increase in M^{II}/M^{III} ratio of Ni-Zn-Mg-Al catalyst having 10 wt.% Ni loading enhanced basic properties of catalysts in terms of both basic site concentration and basic site strength; but only at the cost of Ni dispersion. The Ni-Zn-Mg-Al catalyst of M^{II}/M^{III} ratio = 3.0 (3.0-Cat.) gave the best catalytic performance among the catalysts of varying M^{II}/M^{III} ratio due to the trade-off between basic properties and Ni dispersion. This study further investigates the effect of Ni loading for Ni-Zn-Mg-Al catalysts having M^{II}/M^{III} ratio = 3.0. The CH_4 , CO_2 and H_2O conversions increased significantly on increasing Ni loading from 1.25 wt.% to 5 wt.%. However, these values increased only slightly with further increase in Ni loading to 15 wt.%. Moreover, at 15 wt.% Ni loading, the catalyst underwent coking, resulting in its deactivation. On the other hand, the Ni particles of catalysts having low Ni content (1.25 and 2.5 wt.%) deactivated due to sintering. The catalyst of 5 wt.% Ni loading (5%-Cat) exhibited remarkable stability. In 80 h experimental run at 800°C temperature, 1 atm pressure, feed-stream composition $CH_4:CO_2:H_2O:O_2:N_2 = 1:0.28:0.56:0.08:0.33$ and space velocity of 44743 mL/g.h, the CH_4 , CO_2 and H_2O conversions over 5%-Cat were 78.2%, 80.6% and 70.4% respectively. The negligible drop in CH_4 and CO_2 conversion rates firmly establishes the striking stability of 5%-Cat over 80 h time on stream. Moreover, the average H_2/CO molar ratio of synthesis gas produced in 80 h run was 1.96, quite appropriate for methanol and Fischer-Tropsch synthesis processes.

The kinetic behaviour of 5%-Cat for tri-reforming of methane reaction was investigated in the temperature range of 700°C-800°C with the partial pressure of CH_4 , CO_2 , H_2O and O_2 ranging between 0.47-0.57 atm, 0.03-0.10 atm, 0.08-0.21 atm and 0.007-0.045 atm respectively. Three different elementary reaction steps were assumed to be the rate determining and thus three different Langmuir-Hinshelwood kinetic models were developed. Dual-site mechanism was considered in model development in which CH_4 activates on metallic Ni sites and other co-reactants activate on non-Ni sites of 5%-Cat. The models were optimized using Generalized Reduced Gradient algorithm. The model considering methane dissociation and reaction between adsorbed carbon and adsorbed oxidants as rate determining fitted well with experimental data. The correlation coefficient of parity plot was 0.95. The activation energies of methane cracking and carbon oxidation are calculated to be 111.4 and 206.1 kJ/mol respectively.

सार

ग्लोबल वार्मिंग और जलवायु परिवर्तन वर्तमान सदी की सबसे बड़ी चुनौतियां हैं। ये CO₂ उत्सर्जन से संबंधित होते हैं। CO₂ से ईंधन और रसायनों का रूपांतरण CO₂ उत्सर्जन को रोकने के लिए एक आदर्श रणनीति हो सकती है। इस संदर्भ में, मीथेन का त्रि-सुधार (टी.आर.एम.) एक आशाजनक तकनीक है। CO₂ उत्सर्जन में सबसे बड़ा योगदान इलेक्ट्रिक पावर प्लांटों की गरम धुयें गैस का है। टी.आर.एम. प्रक्रिया को गरम धुयें गैस से CO₂ के पूर्व-पृथक्करण की आवश्यकता नहीं होती है। इस प्रक्रिया में, गरम धुयें गैस के CO₂, H₂O और O₂ संश्लेषण गैस उत्पन्न करने के लिए मीथेन के साथ प्रतिक्रिया करते हैं। हालांकि, उत्प्रेरक का निष्क्रियकरण टी.आर.एम. के बड़े पैमाने पर कार्यान्वयन में बाधा डालता है। उत्प्रेरक कार्बन जमाव, सक्रिय धातु सिंटरिंग और सक्रिय धातु ऑक्सीकरण के कारण निष्क्रिय हो जाते हैं। उत्प्रेरक की उच्च सक्रियता और स्थिरता बनाये रखना टी.आर.एम. की प्रमुख चुनौतियां हैं। इस थीसिस में प्रस्तुत शोध कार्य का उद्देश्य टी.आर.एम. प्रक्रिया में औद्योगिक गरम धुयें गैस के उपयोग के लिए एक अत्यधिक सक्रिय और स्थिर उत्प्रेरक विकसित करना है।

एक उत्प्रेरक के सपोर्ट हिस्सा का उत्प्रेरक प्रदर्शन पर महत्वपूर्ण प्रभाव पड़ता है। Ni उत्प्रेरक के सपोर्ट हिस्सा के रूप में विभिन्न धातु आक्साइड (Al₂O₃, SBA-15, ZrO₂, CeO₂-ZrO₂, TiO₂ और MgO) का उपयोग किया गया था। उनके प्रदर्शन की तुलना समान प्रतिक्रिया में की गई। CH₄ रूपांतरण के आधार पर, इन उत्प्रेरकों की प्रारंभिक सक्रियता इस तरह था: Ni/Al₂O₃ > Ni/SBA-15 > Ni/ZrO₂ > Ni/CeO₂-ZrO₂ > Ni/TiO₂ > Ni/MgO। Ni/Al₂O₃ से प्राप्त Ni/Al₂O₃ में Ni कण अच्छी तरह से छितरे हुए, मजबूत धातु-सपोर्ट इंटरैक्शन, उच्च स्तर की रेड्यूसिबिलिटी और उच्च क्षार उत्पन्न हुई, जिससे अन्य उत्प्रेरकों की तुलना में बेहतर प्रदर्शन किया। तथापि, SBA-15 और ZrO₂ समर्थित Ni उत्प्रेरकों की स्थिरता 10 घंटे रन में उल्लेखनीय रूप से अधिक थी। SBA-15 के हेक्सागोनल झरझरा नेटवर्क ने Ni कणों को समायोजित रखा, जिसके परिणामस्वरूप धातु के सिंटरिंग और कार्बन के जमाव के खिलाफ उच्च प्रतिरोध पैदा हुआ, जबकि Ni/ZrO₂ ने Ni ऑक्सीकरण के लिए अपनी ऑक्सीफिलिक संपत्ति के कारण प्रतिरोध दिखाया। प्रायोगिक जांच से पता चलता है कि Ni/TiO₂ और Ni/MgO ने टी.आर.एम. प्रक्रिया में

कम स्तर की रेड्यूसबिलिटी के कारण कम CH₄, CO₂ और H₂O रूपांतरणों को दिखाया। इसके अलावा, Ni/CeO₂-ZrO₂ उत्प्रेरक ने Ni/Al₂O₃, Ni/SBA-15 और Ni/ZrO₂ की तुलना में बड़े Ni क्रिस्टलीय आकार के कारण निम्न रूपांतरण का प्रदर्शन किया।

Ni/TiO₂, Ni/SBA-15, Ni/MgO, और Ni/Al₂O₃ उत्प्रेरक के प्रदर्शन में धातु-सपोर्ट इंटरैक्शन की भूमिका की जांच की गई। कमजोर धातु-सपोर्ट इंटरैक्शन को लागू करने के लिए, उत्प्रेरक को 400°C पर कैल्सीनेशन किया गया था। जबकि 850°C या उससे अधिक तापमान पर कैल्सीनेशन प्रत्येक उत्प्रेरक में मजबूत धातु-सपोर्ट इंटरैक्शन उत्पन्न किया। Ni/SBA-15 और Ni/Al₂O₃ उत्प्रेरक के लिये मध्यम-शक्ति का धातु-सपोर्ट इंटरैक्शन प्रदान करने के लिए 550°C और 700°C पर कैल्सीनेशन किए गए थे। प्रयोगात्मक परिणामों से पता चला कि Ni/TiO₂ और Ni/MgO उत्प्रेरक जिनके पास कमजोर धातु-सपोर्ट इंटरैक्शन (Ni/TiO₂@400 और Ni/MgO @ 400) था, ने उच्च स्तर की रेड्यूसबिलिटी और Ni फैलाव के कारण उच्च प्रारंभिक सक्रियता प्रदर्शित की। हालाँकि, ये उत्प्रेरक 10 घंटे प्रतिक्रिया रन के दौरान निष्क्रिय हो गए। दूसरी ओर, मजबूत धातु-सपोर्ट इंटरैक्शन से संबंधित Ni/TiO₂ और Ni/MgO उत्प्रेरक का प्रदर्शन (Ni/TiO₂@850 और Ni/MgO@850) असंतोषजनक था। Ni/SBA-15 उत्प्रेरक के लिए, कमजोर धातु-सपोर्ट इंटरैक्शन (Ni/SBA-15@ 400, Ni /SBA-15@550 और Ni/SBA-15@700) वाले उत्प्रेरक अधिक मजबूत धातु-सपोर्ट इंटरैक्शन (Ni/SBA-15@850) वाले उत्प्रेरक से अधिक सक्रिय थे। हालाँकि, Ni/SBA-15 उत्प्रेरकों की स्थिरता धातु-सपोर्ट इंटरैक्शन की ताकत के बजाय SBA-15 के छिद्रों में उपस्थित Ni द्वारा नियंत्रित की गई थी। Ni/Al₂O₃ उत्प्रेरक की सक्रियता में धातु-सपोर्ट इंटरैक्शन की ताकत बढ़ने के साथ (Ni/Al₂O₃@400 < Ni/Al₂O₃@550 < Ni/Al₂O₃@700 < Ni/Al₂O₃@950) वृद्धि पाया गया। मजबूत धातु-सपोर्ट इंटरैक्शन वाले Ni/Al₂O₃ में मोनोडिस्फ़र Ni परमाणु Al₂O₃ के साथ निकट था, जिसके परिणामस्वरूप कमजोर धातु-सपोर्ट इंटरैक्शन वाले Ni/Al₂O₃ की तुलना में उच्च सक्रियता थी। इसके अलावा, निष्क्रियता दर को धातु-सपोर्ट इंटरैक्शन की ताकत में वृद्धि के साथ कम पाया गया क्योंकि मजबूत धातु-सपोर्ट इंटरैक्शन ने कार्बन जमाव और Ni धातु सिंटरिंग के कारण निष्क्रियकरण को कम किया। Ni/Al₂O₃ उत्प्रेरक पर कार्बन जमाव की रासायनिक प्रकृति भी धातु-सपोर्ट इंटरैक्शन की ताकत से प्रभावित हो गई क्योंकि यह धातु-सपोर्ट इंटरैक्शन की ताकत में कमी के साथ अधिक ग्रेफाइटिक बन गया।

टी.आर.एम. प्रक्रिया में उत्प्रेरक के रूप में हाइड्रोटेलेसाइट से प्राप्त सामग्री को भी प्रयोग गया। इस अध्ययन के लिए, पांच उत्प्रेरक तैयार किए गए थे। ये Ni-Mg-Al, Ni-Mg-Al_{me@500}, Ni-Mg-Al_{me@900}, Ni-Cu-Mg-Al और Ni-Zn-Mg-Al थे। Ni-Mg-Al_{me@500} और Ni-Mg-Al_{me@900} को हाइड्रोटेलेसाइट की स्मृति प्रभाव संपत्ति का उपयोग करके संश्लेषित किया गया। Ni-Mg-Al, को कम स्तर की रेड्यूसबिलिटी के कारण कम सक्रिय पाया गया। यद्यपि हाइड्रोटेलेसाइट-व्युत्पन्न Ni उत्प्रेरकों की निर्माण में स्मृति प्रभाव को अपनाने से, रेड्यूसबिलिटी में सुधार हुआ था और Ni-Mg-Al_{me@500} और Ni-Mg-Al_{me@900} के लिए उच्च प्रारंभिक सक्रियता प्राप्त हुई थी, लेकिन ये उत्प्रेरक Ni ऑक्सीकरण, धातु सिंट्रिंग और कार्बन गठन के कारण निष्क्रिय हो गए। Cu के Ni-Mg-Al में जोड़ से Ni-Cu मिश्र धातु का निर्माण हुआ। इसने Ni के कण के आकार को कम कर दिया, जिसके परिणामस्वरूप गैर-प्रवर्तित Ni उत्प्रेरक (Ni-Mg-Al) की तुलना में उच्च सक्रियता और स्थिरता प्राप्त हुई। हालांकि, पोस्ट रिएक्शन परिणामों में Ni-Cu-Mg-Al उत्प्रेरक के Ni ऑक्सीकरण का पता चला। Zn को जोड़ने से इसके धात्विक अवस्था में Ni को बनाए रखने में अधिक प्रभावी पाया गया जिससे इसकी स्थिरता बढ़ गई। इसके अलावा, XPS परिणामों से पता चला है कि Zn ने इलेक्ट्रॉनिक रूप से Ni उत्प्रेरक को चार्ज ट्रांसफर घटना द्वारा संशोधित किया और Ni को इलेक्ट्रॉन समृद्ध बनाया। परिणामस्वरूप, Ni-Zn-Mg-Al उत्प्रेरक ने उल्लेखनीय सक्रियता प्रदर्शित की।

Ni-Zn-Mg-Al उत्प्रेरक का टी.आर.एम. के लिए इसके M_{II}/M_{III} अनुपात और Ni लोडिंग में भिन्नता का अध्ययन किया गया। Ni-Zn-Mg-Al उत्प्रेरक के M_{II}/M_{III} अनुपात में वृद्धि 10 wt% Ni लोडिंग ने क्षार संख्या और क्षार शक्ति दोनों को बढ़ाया; लेकिन Ni फैलाव खराब हो गया। M_{II}/M_{III} अनुपात = 3.0 (3.0-Cat) के Ni-Zn-Mg-Al उत्प्रेरक ने बेहतर क्षार गुणों और बेहतर Ni फैलाव के कारण भिन्न M_{II}/M_{III} अनुपात के उत्प्रेरक की तुलना में सबसे अच्छा प्रदर्शन दिया। यह अध्ययन आगे Ni-Zn-Mg-Al उत्प्रेरक के लिए Ni लोडिंग के प्रभाव की जांच करता है जिसमें M_{II}/M_{III} अनुपात = 3.0 है। CH₄, CO₂ और H₂O रूपांतरण 1.25 wt% से 5 wt% तक Ni लोडिंग बढ़ाने पर काफी बढ़ गए। हालांकि, ये Ni लोडिंग में 15 wt% तक की वृद्धि के साथ केवल थोड़ा बढ़ गए। इसके अलावा, 15 wt% Ni लोडिंग पर, उत्प्रेरक पर अधिक कार्बन जमाव था, जिसके परिणामस्वरूप इसकी निष्क्रिय हो गया। दूसरी ओर, कम Ni लोडिंग (1.25 और 2.5 wt%) वाले उत्प्रेरक के Ni कणों को सिंट्रिंग के कारण निष्क्रिय हो गया। 5 wt% Ni लोडिंग

(5%-कैट) का उत्प्रेरक उल्लेखनीय स्थिरता प्रदर्शित करता है। 80 घंटे रन में 800°C तापमान, 1 atm प्रेशर, फीड-स्ट्रीम कम्पोज़िशन $\text{CH}_4:\text{CO}_2:\text{H}_2\text{O}:\text{O}_2:\text{N}_2 = 1:0.28:0.56:0.08:0.33$ और स्पेस वेलोसिटी 44743 mL/gh पर, यह उत्प्रेरक CH_4 , CO_2 और H_2O रूपांतरण क्रमशः 78.2%, 80.6% और 70.4% दिखाया। 80 घंटे की रन में CH_4 और CO_2 रूपांतरण दरों में नगण्य गिरावट दृढ़ता से 5%-कैट की स्थिरता को स्थापित करती है। इसके अलावा, 80 घंटे रन में निर्मित संश्लेषण गैस का औसत H_2/CO मोलर अनुपात (1.96) मेथनॉल और फिशर-ट्रोप्स संश्लेषण प्रक्रियाओं के लिए काफी उपयुक्त है।

मीथेन की त्रिकोणीय सुधार (टी.आर.एम.) प्रक्रिया के लिए 5%-कैट के गतिज व्यवहार की जांच 700°C-800°C के तापमान सीमा में की गई थी, जिसमें CH_4 , CO_2 , H_2O और O_2 के आंशिक प्रेशर क्रमशः 0.47-0.57 atm, 0.03-0.10 atm, 0.08-0.21 atm और 0.007-0.045 atm थी। तीन अलग-अलग प्राथमिक प्रतिक्रिया चरणों को दर निर्धारण करने वाला माना गया और इस तरह तीन अलग-अलग लैंगमुइर-हिंसेलवुड कैनेटिक मॉडल विकसित किए गए। मॉडल-विकास में दोहरे साइट तंत्र पर विचार किया गया था जिसमें CH_4 धातु Ni साइटों पर सक्रिय होता है और अन्य सह-प्रतिक्रियाकर्ता गैर-Ni साइटों पर सक्रिय होते हैं। मॉडल को सामान्यीकृत-कम-ग्रेडिएंट एल्गोरिथम का उपयोग करके अनुकूलित किया गया था। मीथेन पृथक्करण और कार्बन ऑक्सीकरण को दर निर्धारण करने वाला मॉडल प्रायोगिक डेटा की सही भविष्यवाणी करने में कामयाब रहा। समता भूखंड का सहसंबंध गुणांक 0.95 था। मीथेन पृथक्करण और कार्बन ऑक्सीकरण की सक्रियण ऊर्जा की गणना क्रमशः 111.4 और 206.1 kJ/mol की जाती है।

TABLE OF CONTENTS

	Page No.
Certificate	i
Acknowledgments	iii
Abstract	vii
List of Figures	xv
List of Tables	xxi
Nomenclature	xxiii
CHAPTER 1: INTRODUCTION	1-7
1.1 Background	1
1.2 Tri-reforming of methane	2
1.3 Advantages of Tri-reforming of methane process	3
1.4 Challenges of Tri-reforming of methane process	4
1.5 Objectives	5
1.6 Thesis organization	6
CHAPTER 2: LITERATURE REVIEW	8-47
2.1 Thermodynamics of Tri-reforming of methane	8
2.2 Development of catalysts	10
2.2.1 Role of support on catalytic behavior	11
2.2.2 Role of promoters	21
2.2.3 Influence of catalyst synthesis procedure	24
2.2.4 Effect of metal loading	27
2.3 Reaction operating parameters	29
2.3.1 Effect of feedstock composition	29
2.3.2 Optimization of reaction parameters	41
2.4 Kinetic studies of Tri-reforming of methane reaction	44
2.5 Gaps in literature and motivation for the present work	46
CHAPTER 3: EXPERIMENTAL DETAILS	48-56
3.1 Catalyst preparation	48
3.1.1 Catalyst synthesis for the study of metal oxides as support phase of Ni catalyst	48
3.1.2 Catalyst synthesis for elucidation of role of strength of metal-support interaction of Ni catalyst	49
3.1.3 Catalyst synthesis for the investigation of the performance of hydrotalcite-derived Ni catalysts and the promotional effects of Cu and Zn addition	49
3.1.4 Catalyst synthesis for the study of effect of divalent to trivalent metal ratio (M^{II}/M^{III}) and Ni loading of hydrotalcite-derived Zn-promoted Ni catalyst	50

3.1.5	Catalyst synthesis for kinetic modeling and reaction mechanism study	51
3.2	Catalyst characterization	51
3.3	Catalyst testing	53
3.4	Gaseous product analysis	56
CHAPTER 4: STUDY OF EFFECT OF METAL OXIDES AS SUPPORT PHASE OF Ni CATALYST		57-78
4.1	Catalyst characterization	57
	4.1.1 Characterization of calcined catalysts	57
	4.1.2 Characterization of reduced catalysts	63
	4.1.3 Characterization of used catalysts	67
4.2	Comparison of different catalysts for TRM	71
	4.2.1 Catalyst activity	71
	4.2.2 Catalyst deactivation	75
4.3	Summary of Chapter-4	77
CHAPTER 5: ELUCIDATING THE ROLE OF STRENGTH OF METAL-SUPPORT INTERACTION		79-105
5.1	Catalyst characterization	79
	5.1.1 Ni/TiO ₂ catalyst system	79
	5.1.2 Ni/MgO catalyst system	87
	5.1.3 Ni/Al ₂ O ₃ catalyst system	90
	5.1.4 Ni/SBA-15 catalyst system	95
5.2	Comparison of performance of catalysts having MSI of different strength	100
	5.2.1 Ni/TiO ₂ catalyst system	100
	5.2.2 Ni/MgO catalyst system	103
	5.2.3 Ni/Al ₂ O ₃ catalyst system	103
	5.2.4 Ni/SBA-15 catalyst system	104
5.3	Summary of Chapter-5	105
CHAPTER 6: INVESTIGATION OF THE PERFORMANCE OF HYDROTALCITE-DERIVED Ni CATALYSTS AND THE PROMOTIONAL EFFECTS OF Cu AND Zn ADDITION		106-129
6.1	Catalyst characterization	106
	6.1.1 Characterization of catalyst precursors	106
	6.1.2 Characterization of calcined catalysts	108
	6.1.3 Characterization of reduced catalysts	113
	6.1.4 Characterization of used catalysts	120
6.2	Catalytic tests	124
	6.2.1 Catalytic performance of hydrotalcite-derived catalysts	124
	6.2.2 Catalytic performance of promoted-hydrotalcite-derived catalysts	126
6.3	Summary of Chapter-6	128

CHAPTER 7: STUDY OF EFFECT OF DIVALENT TO TRIVALENT METAL RATIO () AND Ni LOADING OF HYDROTALCITE-DERIVED Zn-PROMOTED Ni CATALYST	130-157
7.1 Catalyst characterization	131
7.1.1 Characterization of catalyst precursors	131
7.1.2 Characterization of calcined catalysts	133
7.1.3 Characterization of reduced catalysts	137
7.1.4 Characterization of used catalysts	144
7.2 Catalytic performance for TRM reaction	149
7.2.1 Effect of M ^{II} /M ^{III} ratio	149
7.2.2 Effect of Ni metal loading	151
7.2.3 Effect of TOS on catalyst stability	153
7.3 Summary of Chapter-7	156
CHAPTER 8: KINETIC MODELING AND REACTION MECHANISM STUDY	158-173
8.1 Kinetic study of Tri-reforming of methane	158
8.1.1 Mass transfer effects and plug flow conditions	158
8.1.2 Effect of partial pressure on reactant's consumption rate and H ₂ /CO molar ratio	160
8.1.3 Effect of temperature and apparent activation energy	166
8.2 Proposed reaction mechanisms	167
8.3 Kinetic rate modeling	168
8.4 Summary of Chapter-8	173
CHAPTER 9: CONCLUSIONS AND RECOMMENDATIONS	174-176
9.1 Conclusions	174
9.2 Recommendations	176
REFERENCES	177-193
APPENDICES	194-207
1 Self-generated figures based on the thermodynamic analysis	194
2 Experimental set-up	196
3 Gas chromatograph calculations	197
4 XRD patterns of catalyst support materials	199
5 Criteria for absence of mass transfer limitations	200
6 Derivation of rate expressions	202
BIODATA	208

LIST OF FIGURES

Fig. No.	Title	Page No.
3.1	Schematic diagram of experimental set-up	54
4.1	XRD patterns of calcined catalysts: (a) Ni/Al ₂ O ₃ , (b) Ni/CeO ₂ -ZrO ₂ , (c) Ni/MgO, (d) Ni/SBA-15, (e) Ni/TiO ₂ and (f) Ni/ZrO ₂	58
4.2	XRD spectra of TiO ₂	59
4.3	SAXS patterns of SBA-15 based samples: (a) SBA-15, (b) calcined Ni/SBA-15, (c) reduced Ni/SBA-15 and (d) used Ni/SBA-15	59
4.4	TPR profiles of calcined catalysts: (a) Ni/Al ₂ O ₃ , (b) Ni/CeO ₂ -ZrO ₂ , (c) Ni/MgO, (d) Ni/SBA-15, (e) Ni/TiO ₂ and (f) Ni/ZrO ₂	60
4.5	TPR profile of NiO	61
4.6	XRD patterns of reduced catalysts: (a) Ni/Al ₂ O ₃ , (b) Ni/CeO ₂ -ZrO ₂ , (c) Ni/MgO, (d) Ni/SBA-15, (e) Ni/TiO ₂ and (f) Ni/ZrO ₂	64
4.7	TEM images of reduced catalysts: (a) Ni/Al ₂ O ₃ , (b) Ni/CeO ₂ -ZrO ₂ , (c) Ni/MgO, (d) Ni/SBA-15, (e) Ni/TiO ₂ and (f) Ni/ZrO ₂	65
4.8	CO ₂ – TPD profiles of reduced catalysts: (a) Ni/Al ₂ O ₃ , (b) Ni/CeO ₂ -ZrO ₂ , (c) Ni/MgO, (d) Ni/SBA-15, (e) Ni/TiO ₂ and (f) Ni/ZrO ₂	66
4.9	NH ₃ – TPD profiles of reduced catalysts: (a) Ni/Al ₂ O ₃ , (b) Ni/CeO ₂ -ZrO ₂ , (c) Ni/MgO, (d) Ni/SBA-15, (e) Ni/TiO ₂ and (f) Ni/ZrO ₂	68
4.10	XRD patterns of used catalysts after 10 h of time on stream study: (a) Ni/Al ₂ O ₃ , (b) Ni/CeO ₂ -ZrO ₂ , (c) Ni/MgO, (d) Ni/SBA-15, (e) Ni/TiO ₂ and (f) Ni/ZrO ₂	69
4.11	TEM images of used Ni/Al ₂ O ₃ catalyst after 10 h of time on stream study	70
4.12	TEM images of used catalysts after 10 h of time on stream study: (a) Ni/Al ₂ O ₃ , (b) Ni/CeO ₂ -ZrO ₂ , (c) Ni/MgO, (d) Ni/SBA-15, (e) Ni/TiO ₂ and (f) Ni/ZrO ₂	71
4.13	Reactant conversions of different catalysts: (a) Ni/MgO, (b) Ni/TiO ₂ , (c) Ni/CeO ₂ -ZrO ₂ , (d) Ni/ZrO ₂ , (e) Ni/SBA-15 and (f) Ni/Al ₂ O ₃ : CH ₄ conversion (A) and CO ₂ conversion (B) as function of time on stream. (reaction conditions: CH ₄ :CO ₂ :H ₂ O:O ₂ :N ₂ = 1:0.23:0.46:0.07:0.28, GHSV = 17220 mLh ⁻¹ g ⁻¹ , Temp. 800°C at 1 atm)	72
4.14	SEM image of used Ni/Al ₂ O ₃ catalyst after 10 h of time on stream study	77
5.1	XRD patterns of Ni/TiO ₂ catalysts: (A) after calcination, (B) after reduction, and (C) after reaction; (a) Ni/TiO ₂ @400, and (b) Ni/TiO ₂ @850	80
5.2	TPR profiles of calcined catalysts: (A) Ni/TiO ₂ , (B) Ni/MgO, (C) Ni/Al ₂ O ₃ , and (D) Ni/SBA-15	81
5.3	TEM images of reduced catalysts: (A) Ni/TiO ₂ @400, (B) Ni/TiO ₂ @850, (C) Ni/MgO@400, (D) Ni/MgO@850, (E) Ni/Al ₂ O ₃ @400, (F) Ni/Al ₂ O ₃ @550, (G) Ni/Al ₂ O ₃ @700, (H) Ni/Al ₂ O ₃ @950, (I) Ni/SBA-15@400, (J) Ni/SBA-15@550, (K) Ni/SBA-15@700 and (L) Ni/SBA-15@850	83

5.4	TEM images of used catalysts after 10 h of time on stream study: (A) Ni/TiO ₂ @400, (B) Ni/TiO ₂ @850, (C) Ni/MgO@400, (D) Ni/MgO@850, (E) Ni/Al ₂ O ₃ @400, (F) Ni/Al ₂ O ₃ @550, (G) Ni/Al ₂ O ₃ @700, (H) Ni/Al ₂ O ₃ @950, (I) Ni/SBA-15@400, (J) Ni/SBA-15@550, (K) Ni/SBA-15@700 and (L) Ni/SBA-15@850	84
5.5	TEM images of used Ni/TiO ₂ @400 catalyst after 10 h of time on stream study	85
5.6	TGA profiles of used catalysts after 10 h of time on stream study: (A) Ni/TiO ₂ , (B) Ni/MgO, (C) Ni/Al ₂ O ₃ , and (D) Ni/SBA-15	86
5.7	NH ₃ – TPD profiles of TiO ₂ and Ni/TiO ₂ catalysts: (a) TiO ₂ , (b) Ni/TiO ₂ @850, and (c) Ni/TiO ₂ @400	87
5.8	XRD patterns of Ni/MgO catalysts: (A) after calcination, (B) after reduction, and (C) after reaction; (a) Ni/MgO@400, and (b) Ni/MgO@850	88
5.9	CO ₂ – TPD profiles of Ni/MgO catalysts: (a) Ni/MgO@400, and (b) Ni/MgO@850	90
5.10	XRD patterns of Ni/Al ₂ O ₃ catalysts: (A) after calcination, (B) after reduction, and (C) after reaction; (a) Ni/Al ₂ O ₃ @400, (b) Ni/Al ₂ O ₃ @550, (c) Ni/Al ₂ O ₃ @700, and (d) Ni/Al ₂ O ₃ @950	91
5.11	NH ₃ – TPD profiles of Ni/Al ₂ O ₃ catalysts: (a) Ni/Al ₂ O ₃ @400, (b) Ni/Al ₂ O ₃ @550, (c) Ni/Al ₂ O ₃ @700, and (d) Ni/Al ₂ O ₃ @950	93
5.12	Raman spectra of used Ni/Al ₂ O ₃ catalysts after 10 h of time on stream study	95
5.13	XRD patterns of Ni/SBA-15 catalysts: (A) after calcination, (B) after reduction, and (C) after reaction; (a) Ni/SBA-15@400, (b) Ni/SBA-15@550, (c) Ni/SBA-15@700, and (d) Ni/SBA-15@850	96
5.14	A) N ₂ physisorption isotherms and (B) Pore size distributions of parent SBA-15, calcined Ni/SBA-15@400, calcined Ni/SBA-15@550, calcined Ni/SBA-15@700 and calcined Ni/SBA-15@850	97
5.15	CO ₂ – TPD profiles of Ni/SBA-15 catalysts: (a) Ni/SBA-15@400, and (b) Ni/SBA-15@850	100
5.16	CH ₄ conversion as a function of time on stream: (A) Ni/TiO ₂ , (B) Ni/MgO, (C) Ni/Al ₂ O ₃ , and (D) Ni/SBA-15. (reaction conditions: CH ₄ :CO ₂ :H ₂ O:O ₂ :N ₂ = 1:0.23:0.46:0.07:0.28, space velocity = 17220 mLh ⁻¹ g ⁻¹ , Temp. 800°C at 1 atm)	101
5.17	CO ₂ conversion as function of time on stream: (A) Ni/TiO ₂ , (B) Ni/MgO, (C) Ni/Al ₂ O ₃ , and (D) Ni/SBA-15. (reaction conditions: CH ₄ :CO ₂ :H ₂ O:O ₂ :N ₂ = 1:0.23:0.46:0.07:0.28, space velocity = 17220 mLh ⁻¹ g ⁻¹ , Temp. 800°C at 1 atm)	102
6.1	XRD patterns of dried Mg-Al and catalyst precursors: (a) Mg-Al, (b) Ni-Mg-Al (c) Ni-Mg-Al_me@900, (d) Ni-Mg-Al_me@500, (e) Ni-Cu-Mg-Al and (f) Ni-Zn-Mg-Al	107
6.2	XRD patterns of calcined samples: (a) calcined at 500°C before dipping in aqueous Ni(II) nitrate solution, and (b) calcined at 900°C before dipping in aqueous Ni(II) nitrate solution	108
6.3	XRD patterns of calcined catalysts: (a) Ni-Mg-Al (b) Ni-Mg-Al_me@900, (c) Ni-Mg-Al_me@500, (d) Ni-Cu-Mg-Al and (e) Ni-Zn-Mg-Al	109

6.4	TPR profiles of calcined catalysts: (a) Ni-Mg-Al (b) Ni-Mg-Al_me@900, (c) Ni-Mg-Al_me@500, (d) Ni-Cu-Mg-Al and (e) Ni-Zn-Mg-Al	110
6.5	SEM images of dried catalyst precursors: (a) Ni-Mg-Al_me@500, (b) Ni-Mg-Al_me@900 and (c) Ni-Mg-Al	112
6.6	XRD patterns of reduced catalysts: (a) Ni-Mg-Al (b) Ni-Mg-Al_me@900, (c) Ni-Mg-Al_me@500, (d) Ni-Cu-Mg-Al and (e) Ni-Zn-Mg-Al	114
6.7	CO ₂ – TPD profiles of reduced catalysts: (a) Ni-Mg-Al (b) Ni-Mg-Al_me@900, (c) Ni-Mg-Al_me@500, (d) Ni-Cu-Mg-Al and (e) Ni-Zn-Mg-Al	116
6.8	NH ₃ – TPD profiles of reduced catalysts: (a) Ni-Mg-Al (b) Ni-Mg-Al_me@900, (c) Ni-Mg-Al_me@500, (d) Ni-Cu-Mg-Al and (e) Ni-Zn-Mg-Al	117
6.9	TEM images of reduced catalysts: (a) Ni-Mg-Al (b) Ni-Mg-Al_me@900, (c) Ni-Mg-Al_me@500, (d) Ni-Cu-Mg-Al and (e) Ni-Zn-Mg-Al	118
6.10	XPS spectra of reduced catalysts: (a) Ni-Mg-Al (b) Ni-Cu-Mg-Al and (c) Ni-Zn-Mg-Al	119
6.11	XRD patterns of used catalysts after 20 h of time on stream study: (a) Ni-Mg-Al (b) Ni-Mg-Al_me@900, (c) Ni-Mg-Al_me@500, (d) Ni-Cu-Mg-Al and (e) Ni-Zn-Mg-Al	120
6.12	TGA profiles of used catalysts after 20 h of time on stream study: (a) Ni-Mg-Al (b) Ni-Mg-Al_me@900, (c) Ni-Mg-Al_me@500, (d) Ni-Cu-Mg-Al and (e) Ni-Zn-Mg-Al	122
6.13	TPO profiles of reduced catalysts: (a) Ni-Mg-Al (b) Ni-Cu-Mg-Al and (c) Ni-Zn-Mg-Al	122
6.14	TEM images of used catalysts after 20 h of time on stream study: (a) Ni-Mg-Al (b) Ni-Mg-Al_me@900, (c) Ni-Mg-Al_me@500, (d) Ni-Cu-Mg-Al and (e) Ni-Zn-Mg-Al	123
6.15	Reactant conversion (%) of different catalysts: (a) Ni-Mg-Al (b) Ni-Mg-Al_me@500, (c) Ni-Mg-Al_me@900, (d) Ni-Cu-Mg-Al and (e) Ni-Zn-Mg-Al: CH ₄ conversion % (A) and CO ₂ conversion % (B) as function of time on stream. (reaction conditions: CH ₄ :CO ₂ :H ₂ O:O ₂ :N ₂ = 1:0.23:0.46:0.07:0.28, SV = 49200 mLh ⁻¹ g ⁻¹ , Temp. 800°C at 1 atm)	125
7.1	XRD patterns of dried catalyst precursors: (A) dried samples of different M ^{II} /M ^{III} ratio and (B) dried samples of different Ni loading	132
7.2	XRD patterns after calcination: (A) calcined samples of different M ^{II} /M ^{III} ratio and (B) calcined samples of different Ni loading	134
7.3	TPR profiles: (A) calcined samples of different M ^{II} /M ^{III} ratio and (B) calcined samples of different Ni loading	136
7.4	XRD patterns after in situ reduction: (A) reduced samples of different M ^{II} /M ^{III} ratio and (B) reduced samples of different Ni loading	139
7.5	CO ₂ – TPD profiles: (A) reduced samples of different M ^{II} /M ^{III} ratio and (B) reduced samples of different Ni loading	141
7.6	NH ₃ – TPD: (A) reduced samples of different M ^{II} /M ^{III} ratio and (B) reduced samples of different Ni loading	142

7.7	TEM images of reduced samples: (a) 2.0-R, (b) 2.5-R, (c) 3.0-R, (d) 3.5-R, (e) 1.25%-R, (f) 2.5%-R, (g) 5%-R and (h) 15%-R	143
7.8	XRD patterns after 20 h of time on stream study: (A) used samples of different M^{II}/M^{III} ratio and (B) used samples of different Ni loading	145
7.9	TGA profiles after 20 h of time on stream study: (A) used samples of different M^{II}/M^{III} ratio and (B) used samples of different Ni loading	146
7.10	TEM images of used samples after 20 h of time on stream study: (a) 2.0-U, (b) 2.5-U, (c) 3.0-U, (d) 3.5-U, (e) 1.25%-U, (f) 2.5%-U, (g) 5%-U and (h) 15%-U	147
7.11	TEM images of 15%-U catalyst after 20 h run	148
7.12	Reactant conversion (%) of catalysts having different M^{II}/M^{III} ratio: (A) CH_4 conversion (%) and (B) CO_2 conversion (%) as function of time on stream. (reaction conditions: $CH_4:CO_2:H_2O:O_2:N_2 = 1:0.23:0.46:0.07:0.28$, $SV = 49200 \text{ mLh}^{-1}\text{g}^{-1}$, Temp. 800°C at 1 atm)	150
7.13	Reactant conversion (%) of catalysts having different Ni loading: (A) CH_4 conversion (%) and (B) CO_2 conversion (%) as function of time on stream. (reaction conditions: $CH_4:CO_2:H_2O:O_2:N_2 = 1:0.23:0.46:0.07:0.28$, $SV = 49200 \text{ mLh}^{-1}\text{g}^{-1}$, Temp. 800°C at 1 atm)	152
7.14	CH_4 and CO_2 conversion (%) of 5%-Cat as function of time on stream. (reaction conditions: $CH_4:CO_2:H_2O:O_2:N_2 = 1:0.28:0.56:0.08:0.33$, $SV = 44743 \text{ mLh}^{-1}\text{g}^{-1}$, Temp. 800°C at 1 atm)	153
7.15	TGA profile of 5%-U catalyst after 80 h run	154
7.16	XRD pattern of 5%-U catalyst after 80 h run	155
7.17	TEM image of 5%-U catalyst after 80 h run	155
8.1	Effect of feed volumetric flowrate on methane conversion at 700°C temperature, 1 atm pressure and $W/F = 9.77 \text{ g}_{\text{cat.}}\text{s/L @ STP}$	159
8.2	Effect of catalyst particle size on methane conversion at 700°C temperature, 1 atm pressure and $W/F = 9.77 \text{ g}_{\text{cat.}}\text{s/L @ STP}$	159
8.3	Effect of partial pressure of methane on CH_4 , CO_2 , and H_2O conversions and H_2/CO molar ratio at 750°C temperature, 1 atm pressure and $W/F = 9.77 \text{ g}_{\text{cat.}}\text{s/L @ STP}$	161
8.4	Effect of partial pressure of methane on CH_4 , CO_2 , and H_2O conversions at different temperatures and at 1 atm pressure and $W/F = 9.77 \text{ g}_{\text{cat.}}\text{s/L @ STP}$	162
8.5	Effect of CO_2 partial pressure on CH_4 , CO_2 , and H_2O conversions and H_2/CO molar ratio at 750°C temperature, 1 atm pressure and $W/F = 9.77 \text{ g}_{\text{cat.}}\text{s/L @ STP}$	163
8.6	Effect of H_2O partial pressure on CH_4 , CO_2 , and H_2O conversions and H_2/CO molar ratio at 750°C temperature, 1 atm pressure and $W/F = 9.77 \text{ g}_{\text{cat.}}\text{s/L @ STP}$	164
8.7	Effect of O_2 partial pressure on CH_4 , CO_2 , and H_2O conversions and H_2/CO molar ratio at 750°C temperature, 1 atm pressure and $W/F = 9.77 \text{ g}_{\text{cat.}}\text{s/L @ STP}$	165
8.8	Effect of reaction temperature on CH_4 , CO_2 , and H_2O consumption rates and H_2 and CO formation rates at 1 atm pressure, $CH_4:CO_2:H_2O:O_2:N_2 = 1:0.28:0.56:0.08:0.33$ and $W/F = 9.77 \text{ g}_{\text{cat.}}\text{s/L @ STP}$	166

8.9	Effect of temperature on adsorption equilibrium constants (K_1 , K_3 , K_4 and K_5) and rate constants (k_2 and k_6) for model 3	172
8.10	Statistical fit of the postulated kinetic rate model 3 showing comparison between the predicted rates and the experimental rates	172

LIST OF TABLES

Table No.	Title	Page No.
2.1	Summary of studies reporting catalyst development	12
2.2	Summary of studies reporting effect of reaction operating parameters	31
3.1	Experimental conditions for tri-reforming of methane reaction	55
4.1	Physicochemical properties of catalysts	62
4.2	BET surface area, pore volume and average pore diameter of catalyst supports	63
4.3	Physicochemical properties of used catalysts after 10 h of time on stream study	68
4.4	Activity data of catalysts for TRM (reactions conditions: CH ₄ :CO ₂ :H ₂ O:O ₂ :N ₂ = 1:0.23:0.46:0.07:0.28, GHSV = 17220 mLh ⁻¹ g ⁻¹ , Temp. 800°C at 1 atm)	73
5.1	Physicochemical properties of catalysts	82
5.2	Acid sites concentration of Ni/Al ₂ O ₃ catalysts calcined at different temperatures	93
5.3	Textural properties of parent SBA-15 and SBA-15 supported calcined Ni catalysts	98
5.4	Activity data of different catalysts for TRM (reactions conditions: CH ₄ :CO ₂ :H ₂ O:O ₂ :N ₂ = 1:0.23:0.46:0.07:0.28, space velocity = 17220 mLh ⁻¹ g ⁻¹ , Temp. 800°C at 1 atm)	102
6.1	Physicochemical properties of catalysts	110
6.2	Metal compositions of reduced catalysts	114
6.3	Physicochemical properties of used catalysts after 20 h of time on stream study	121
6.4	Activity data of different catalysts for TRM (reactions conditions: CH ₄ :CO ₂ :H ₂ O:O ₂ :N ₂ = 1:0.23:0.46:0.07:0.28, SV = 49200 mLh ⁻¹ g ⁻¹ , Temp. 800°C at 1 atm)	126
7.1	Notations of catalyst samples	130
7.2	d-spacing of (110) and (003) peaks of XRD patterns of dried catalyst precursors	133
7.3	Amount of H ₂ consumption in TPR analysis	135
7.4	Physicochemical properties of catalysts	137
7.5	Metal compositions of reduced catalysts	137
7.6	Physicochemical properties of used catalysts after 20 h of time on stream study	144
7.7	Activity data of different catalysts for TRM (reactions conditions: CH ₄ :CO ₂ :H ₂ O:O ₂ :N ₂ = 1:0.23:0.46:0.07:0.28, SV = 49200 mLh ⁻¹ g ⁻¹ , Temp. 800 °C at 1 atm)	151
7.8	Comparison of performance of catalyst developed in present study with performances of catalysts reported in literature	156
8.1	Comparison of apparent activation energy (E _{app} , kJ/mol) over Ni-based catalysts	167
8.2	Kinetic model parameters	170

8.3	Evaluation of thermodynamic relevance of the adsorption constants of Model 3
-----	--

171

NOMENCLATURE

d	d-spacing	nm
D	Internal diameter of reactor	mm
D_p	Average catalyst particle size	nm
D_{pore}	Mesopore size	nm
E_{app}	Apparent activation energy	
F	Volumetric flow rate of feed	L/s
K_1	Adsorption constant of CH ₄	atm ⁻¹
k_2	Rate constant of methane decomposition reaction	mol.g ⁻¹ s ⁻¹
K_3	Adsorption constant of CO ₂	atm ⁻¹
K_4	Adsorption constant of H ₂ O	atm ⁻¹
K_5	Adsorption constant of O ₂	atm ⁻¹
k_6	Rate constant of reaction between adsorbed carbon and adsorbed oxidants	
L	Height of catalyst bed	cm
S_{BET}	Total surface area	m ² /g
S_{meso}	Mesopore surface area	m ² /g
S_{micro}	Micropore surface area	m ² /g
V_{micro}	Micropore volume	cm ³ /g
W	Weight of catalyst	G
ΔH	Change in enthalpy	J/mol.K
ΔS	Change in entropy	J/mol

Greek letters

λ	X-ray wavelength	Å
β	Full width at half maximum	Å
θ	Peak position	°

Subscripts

i	Reactant or product species
---	-----------------------------

Acronyms

atm	Atmosphere
BET	Brunauer–Emmett–Teller
BJH	Barrett-Joyner-Halenda
CCS	Carbon capture and sequestration
CCU	Carbon capture and utilization
CNT	Carbon nanotube
DRM	Dry reforming of methane
EDX	Energy dispersive X-ray
ev	Electron volt
FWHM	Full width at half maximum
GHSV	Gas hourly space velocity
h	Hour
HTlc	Hydrotalcite-like compound
JCPDS	Joint Committee on Powder Diffraction Standards
me	Memory effect
M ^{II} /M ^{III} ratio	Divalent to trivalent metal molar ratio
MMSI	Medium metal-support interactions
MP-AES	Microwave plasma atomic emission spectroscopy
MSI	Metal-support interactions
nm	Nanometer
POM	Partial oxidation of methane
PSD	Particle size distribution
RDS	Rate determining step
RMSE	Root mean square error
RWGS	Reverse water-gas shift
SAXS	Small angle X-ray scattering
SEM	Scanning electron spectroscopy
SMSI	Strong metal-support interactions
SRM	Steam reforming of methane
STP	Standard temperature and pressure
TCD	Thermal conductivity detector
TEM	Transmission electron spectroscopy
TEOS	Tetraethyl orthosilicate
TGA	Thermo-gravimetric analysis
TOS	Time on stream
TPD	Temperature programmed desorption
TPO	Temperature programmed oxidation
TPR	Temperature programmed reduction
TRM	Tri-reforming of methane
WMSI	Weak metal-support interactions
XPS	X-ray photoelectron spectroscopy
XRD	X-ray diffraction